Characterization of Vegetation with Combined Thematic Mapper (TM) and Shuttle Imaging Radar (SIR-B) Image Data

Jack F. Paris and *Helenann H. Kwong*
Jet Propulsion Laboratory, California Institute of Technology, Pasadena, CA 91109

ABSTRACT: Based on TM and SIR-B image data for Fresno County, California, in October 1984, we found that the sensors provided quantitative information on the amounts of herbaceous and woody vegetation in a given field. Optical reflectance spectra responded primarily to green, foliar biomass, and L-band (23-cm) backscattering coefficients related primarily to standing, woody biomass. A simple progressive transformation of the concatenated spectra produced three continuous measures of biophysical condition, F_1, F_2, and F_3. These indicated the percent ground cover, the green leaf-area index (or standing green biomass per unit area), and the woody biomass per unit area, respectively.

INTRODUCTION

Remote sensing of some of the biophysical characteristics of terrestrial vegetation on a global scale from Earth-orbiting spacecraft promises to provide valuable information for ecologists, climatologists, hydrologists, and vegetation resource managers. For example, the condition of the terrestrial biosphere influences the flux of energy (radiation and latent and sensible heat), of momentum (drag), and of masses (e.g., water, nutrients, oxygen, and carbon dioxide) between the biosphere and the atmosphere (Sellars *et al.*, 1986). Measurements of the state of the biosphere and its change over time bear directly on important issues related to deforestation, carbon cycling, acid deposition, and air pollution. In addition, global botanical information is useful in economic matters such as surveying the state of food and fiber resources.

Many investigators have studied the information content of optical data with a heavy concentration on Landsat sensors [i.e., the Multispectral Scanner (MSS) and the Thematic Mapper (TM)]. The remote sensing and botanical literature is filled with papers on the potential or actual uses of MSS and TM image data (see Colwell (1983) for a summary). Other investigators have explored the information content of active-microwave data (see Ulaby *et al.* (1983) for a summary). Few researchers have treated the combined uses of optical and active-microwave data for characterization of vegetation (Wu, 1981). In this paper, we present the results of our study of combined optical and active-microwave image data from spacecraft over a region in California having a wide variety of herbaceous and woody vegetation.

In October 1984, the National Aeronautics and Space Administration (NASA) conducted the second of a series of Shuttle Imaging Radar (SIR) missions. The first mission (SIR-A) was completed in November 1981. It was a synthetic aperture radar (SAR) that operated in the L-band at a wavelength of 23.5 cm with horizontal polarization for both microwave transmission and reception (i.e., HH polarization combination). SIR-A viewed the Earth's surface at an incidence angle of about 50 degrees (measured on the surface). The SIR-A mission was brief and covered some land areas between 38°N and 38° S latitude. The quality of the SIR-A data was somewhat poor due to the relatively coarse 40-m spatial resolution (six looks) and the optical processing of the signal data to produce images. Previous to the SIR-A mission during the summer of 1978 (8 July to 10 October), NASA had acquired SAR data from the polar-orbiting Seasat. It operated at 23.5 cm, with the HH polarization combination, and with an incidence angle at the surface of about 20 degrees. The quality of the Seasat SAR data was excellent with a 25-m spatial resolution (four looks) and digital processing of the signal data to produce images. Also, the sensor obtained the only truly multidate spacecraft-based SAR data set.

The primary differences between the SIR-B mission and previous spacecraft-borne SAR missions were (1) the ability to select an incidence angle between about 15 and 60 degrees and (2) the inclusion of 12 vegetation investigations. The other SIR-B sensor characteristics were about the same as those of the Seasat SAR and SIR-A (i.e., 23.5 cm and HH). The latitude range of the SIR-B was between 57°N and 57°S, which was midway between the ranges of Seasat and SIR-A. Before the beginning of the mission, the quality of the SIR-B had been expected to be similar to that of the Seasat SAR (25-m spatial resolution with four looks and digital processing).

As one of the 43 SIR-B investigators, we conducted our SIR-B experiment at a test site in Fresno County, California, centered on Raisin City. We had used the site for several airborne SAR (ASAR) experiments starting in March 1984, and continuing to July 1985, when the ASAR was destroyed in a fire aboard the NASA Convair 990 aircraft. Thus, we had collected a continuing set of ground-based measurements that enabled us to describe at least some important aspects of the biophysical characteristics of the fields. The site contained a wide variety of herbaceous and woody plants under cultivation as a part of the thriving commercial agriculture of the San Joaquin Valley in California. Due to the favorable climate, the growing season in the Valley is quite long compared to many other regions in the United States. The main herbaceous crops present at the time of the SIR-B overflight were alfalfa, corn, cotton, and some vegetable crops (e.g., blackeyes and carrots). The main woody plants were various deciduous nut and fruit orchards (almonds, walnuts, pecans, peaches, plums) and various vineyards. These existed with different substrate conditions, including wet and dry soils, flooded fields (irrigation), and various amounts of ground cover by herbaceous ground plants. In addition, in October, many woody plants and herbaceous plants were undergoing different stages of senescence. Thus, the woody plants had a variety of herbaceous and woody components during the SIR-B mission.

In the early morning of 9 October 1984, the SIR-B acquired signal data at an incidence angle of 40 degrees. On 10 October, the SIR-B repeated its coverage at an incidence angle of 22 degrees. An earlier attempt at 50 degrees on 8 October was aborted when problems developed in acquiring the Tracking and Data Relay System Satellite (TDRSS) during the overpass. When we received the two successful SIR-B images, we found that the 40-degree data had partly missed the test site and had included

PHOTOGRAMMETRIC ENGINEERING AND REMOTE SENSING,
Vol. 54, No. 8, August 1988, pp. 1187–1193.

0099-1112/88/5408–1187$02.25/0

only the southeastern half. In addition, due to transmitter problems, the signal-to-noise ratio of the 40-degree data (being acquired over a longer path length than the 22-degree data) was quite low (Cimino *et al.*, 1986a). The result of these circumstances led us to concentrate on the 22-degree SIR-B data.

For the optical portion of our study, we used a Thematic Mapper (TM) image acquired over the test site under cloud-free conditions on 5 October 1984. The TM operates in six reflective-wavelength bands (see Table 1) and acquires image data having excellent quality with a 30-m spatial resolution. Thus, the basic spacecraft-based image data set for our study consisted of the TM data acquired in mid-morning on 5 October and the SIR-B 22-degree data acquired just before dawn on 10 October. To support these data, we had collected ground-based information on 2, 8, 9, and 10 October. We interpolated these where appropriate to estimate conditions on 5 October, the date of the TM coverage. With these data, we could investigate the nature of the TM spectra and SIR-B backscattering to ascertain the effects of various biophysical conditions on these.

The findings of this study serve to define hypotheses that investigators can use in the future or in other places with existing data sets as part of the scientific questions that they can address. Hopefully, the research community can arrive at a set of working hypotheses that will be the basis of operational sensing in the coming Earth Observation system (Eos) era.

MATERIALS AND METHODS

DATA PREPARATION FOR ANALYSIS

Both SIR-B and TM data exist in uncalibrated formats. Thus, the first task was to register the SIR-B data to the TM data. We used the PICCCA software package written by C. C. Davis of the Jet Propulsion Laboratory (JPL) to perform this task on the Multimission Image Processing Laboratory (MIPL) VAX 11/780 and VAX 8600 at JPL. Because the test site is quite level, the use of road intersections for tie points produced an excellent registration accuracy (mean pixel location error of 0.3 for tie points). Due to the combination of poor signal-to-noise in the SIR-B image and the natural variability from pixel to pixel due to the well-known effects of fading (image speckle), the registration of the SIR-B image set to the TM data set was essential to the next step – the extraction of field averages. We could easily locate a subject field in a selected channel of the TM. Then, we could extract all of the concatenated data (TM and SIR-B) from that field for all bands including the SIR-B.

To extract field average brightnesses (digital number, N_{ij}) for the ith sensor band ($i = 1$ to 7 for the TM and $i=8$ for SIR-B) and the jth field, we used the Aries III Image Analysis System with the DIPIX software on the VAX 11/750 belonging to the Geology Group at JPL. With extracted field average data, we could have proceeded with standard maximum likelihood operations to classify the concatenated data set. However, we were interested in creating a transformation that presented the concatenated data as a set of continuous measures of biophysical condition rather than as categories. To pursue this direction of research, we first converted the uncalibrated data to calibrated reflectance factors.

TABLE 1. REFLECTIVE SPECTRAL BANDS OF THE LANDSAT THEMATIC MAPPER.

Band Number	Wavelength Definition (μm)
1	0.45 – 0.52
2	0.52 – 0.60
3	0.63 – 0.69
4	0.76 – 0.90
5	1.55 – 1.75
7	2.09 = 2.38

For the SIR-B data, we had access to a set of calibration equations and parameters that Dr. James Wang of the Goddard Space Flight Center (GSFC) had developed for his SIR-B experiment in parts of Fresno County to the southwest and to the northeast of our Raisin City Test Site. See Wang *et al.* (1986) and Dobson *et al.* (1986) for a full discussion of this technique of calibration. This produces estimates of the backscattering coefficient, σ^o, from the original digital number data. Radar engineers usually express σ^o in decibels (i.e., as the logarithm of σ^o). In our study, to place the SIR-B data on a par with TM data, we expressed the backscattering data in terms of reflectance factor, R (percent), which is the backscattering of the object under study compared to that of a perfectly diffuse and non-absorbing level surface. The conversion from σ^o to R is

$$R = 25\ \sigma^o/\mu^2 \qquad (1)$$

where μ is the cosine of the incidence angle. Here, of course, σ^o is expressed as the backscattering cross section (m^2) of the object per horizontal area (m^2) of the extended-area object.

For the optical bands of the concatenated data, we used a simple scheme to convert N to R. In the TM scene, a pond and several bare fields existed. By assigning a reasonable set of reflectance-factor values (one for each band) to the pond (dark) and to a selected bare field (bright) and by using the N values for these (in each band), we developed a linear transform to convert N-values to R-values. We used a separate equation for each TM band. We then applied these transformations to all of the fields to produce estimates of reflectance factors of each field in each band. The set of reflectance factors then became the reflectance spectra for the field. With the reflectance factor from the SIR-B, we produced the concatenated reflectance spectra for each field. For our purposes, we only wanted to produce estimates of reflectance having first-order accuracies. Because all of our subsequent transformations were linear, small errors in the calibration process would be unimportant. We desired calibrated values of spectra to allow us (1) to compare TM/SIR-B spectra directly to calibrated field measurements for the same types of objects and (2) to give meaning to representation of spectral differences as Euclidian distances in multidimensional feature space (see following sections). We performed all of the calibration operations on extracted field-averaged data on a desktop computer with a spreadsheet/graphics program.

GROUND-BASED MEASUREMENTS AND OBSERVATIONS

Starting in March 1984, we had been collecting a number of different measures of biophysical condition in several hundred fields in the Raisin City Test Site. These were to support both an on-going series of ASAR experiments and the SIR-B/TM. Due primarily to the limitations of funding (and hence personnel) and to the need to collect concurrent data (on a given date of remotely sensed data acquisition) for several hundred fields during a few hours, we chose to use simple, non-destructive methods of sampling as follows.

For row crops, such as cotton and corn, we measured the row spacing and plant density (number per row). We recorded the row direction; because SIR-B viewed the scene toward the northwest, and because all rows ran either north-south or east-west, the row direction did not affect the SIR-B measurements. For the TM, with the solar azimuth toward the southeast, the space between rows could be illuminated for crops having east-west rows. This fact is the basis for using east-west rows for raisin grapes where growers dry the grapes in the sun by placing the grapes on paper trays on the ground between the rows. For the cotton, we noted a categorical indication of the defoliation state. In the fall, growers use aerial spraying of defoliation agents to produce a defoliated crop that can be harvested. For alfalfa, we measured the standing height, h (cm), of the alfalfa at several points in the field near the edge of the field. In addition, we noted the general quality condition of the alfalfa in terms of uniformity of cover and percent weeds. For orchards, we collected a set of data giving the height of the trees, the circumference of the trunk (at a height of 30 cm because the trees branched near the ground), the spacing between the rows, and the spacing between the trees along a row. On the dates of the experiments, we noted the general condition of the substrate (soil moisture in a categorical manner) and of the foliage. We took 35-mm photographs (ordinary color) of many fields on the dates of sensor-data acquisition. We compiled these data into a spreadsheet/database worksheet by field number so that we could combine these with the extracted and transformed data from the SIR-B and TM.

Progressive Transformation of Concatenated Spectra

An important difference between the our approach and standard image analyses is our emphasis on the extraction of continuous measures of biophysical condition. These measures are derived from calibrated concatenated spectra (TM plus SIR-B) through the use of mathematical operations that yield a number of scalar measures that bear orthogonal relationships to each other. We refer to these measures as features, F_k ($k = 1$ to M). In the history of remote sensing investigations, many scientists have defined transformations involving two or more bands to produce scalar measures of condition. For example, the vegetation index, ν, is often used [where ν is the ratio of the near-infrared reflectance factor (R_4) to the red-light reflectance factor (R_3)]. Another popular transformation is the normalized difference, N, between R_4 and R_3 (Tucker, 1979). The literature is full of transformations intended for use with optical data (see Perry and Lautenschlager (1984) for a summary and interesting comments on the interrelationship among these). Some investigators have used all MSS or TM bands to produce orthogonal, scalar measures of the biophysical condition of vegetation (Kauth and Thomas, 1976; Crist and Cicone, 1984). We follow the spirit of these transformations in our treatment of the transformation of concatenated spectra. However, we applied a simple progressive transformation method that differs from principal components analysis. The progressive transformation method operates as follows.

We view the concatenated spectra as points in multi-dimensional feature (reflectance-factor) space with the number of coordinate axes equal to the number of sensor bands. We represent a spectra as a column vector, $\mathbf{R}$, where

$$\mathbf{R} = [R_1\ R_2\ R_3 R_4\ R_5\ R_7\ R_8]^T \qquad (2)$$

The subscripts refer to the various bands of TM with Band 8 being the SIR-B 22-degree incidence-angle band.

Before we proceeded with the translation and rotation of feature space in the progressive transformation operations, we elevated the importance of the single SIR-B band by multiplying R_8 values by a factor of 10. This placed the single band of SIR-B on a better par with the six-bands of TM and produced a range in R_8 that was similar to that of the actively-changing TM bands. Such rescaling of reflectance is important because the measure of spectral difference is the Euclidian distance in 7-space. We refer to the modified coordinate system as System 1.

The first operation of the progressive transformation procedure is the selection of a spectrum ($\mathbf{R}_B$) that defines a new origin of a translated coordinate system, System 2. In System 2, the concatenated spectra, $\mathbf{S}$, are obtained by

$$\mathbf{S} = \mathbf{R} - \mathbf{R}_B \qquad (3)$$

The second operation is the selection of a spectrum, $\mathbf{S}_1$, that represents some biophysical condition of interest. $\mathbf{S}_1$ comes from $\mathbf{R}_1$ through the first operation (Equation 1). Ideally, one would want to pick $\mathbf{R}_B$ and $\mathbf{R}_1$ to indicate the direction of change in spectra in multi-dimensional feature space due to some selected biophysical-condition difference between these two spectra. The analyst controls the nature of the extracted information through his or her selection of reference spectra.

The direction of $\mathbf{S}_1$ is indicated by a unit vector, $\mathbf{f}_1$ which is obtained by the usual vector operation of division by the magnitude of the vector. The first coordinate axis of the translated and rotated coordinate System 3 is represented by $\mathbf{f}_1$. To find the projection (scalar measure, F_1) of $\mathbf{S}$ along $\mathbf{f}_1$, use the vector dot product,

$$F_1 = \mathbf{f} \cdot \mathbf{S}. \qquad (4)$$

At this point in the process, one may calculate the maximum distance that a given spectrum lies from the first coordinate axis. We call this the first residual distance, D_1, where

$$D_1 = (|\mathbf{S}|^2 - F_1^2)^{0.5}. \qquad (5)$$

The third operation is the selection of another spectrum, $\mathbf{S}_2$, to represent another biophysical condition in contrast to those represented by $\mathbf{R}_B$ (or $\mathbf{S}_B = \mathbf{0}$) and $\mathbf{S}_1$. In general, one would not expect $\mathbf{S}_2$ to be orthogonal to $\mathbf{S}_1$. Thus, we used the vector properties of $\mathbf{S}_2$ and $\mathbf{f}_1$ to define a vector. $\mathbf{F}_2$, such that the associated unit vector, $\mathbf{f}_2$, is orthogonal to $\mathbf{f}_1$. One valid expression for $\mathbf{F}_2$ is

$$\mathbf{F}_2 = \mathbf{S}_2 - (\mathbf{f}_1 \cdot \mathbf{S}_2)\ \mathbf{F}_1. \qquad (6)$$

The projection (scalar measure, F_2) of any spectrum along $\mathbf{f}_2$ is obtained in a manner to that of $\mathbf{f}_1$. With F_1 and F_2, one can calculate the second residual distance, D_2, which represents the distance between the spectrum and the plane defined by $\mathbf{f}_1$ and $\mathbf{f}_2$.

In the remaining operations, we selected spectra to represent other biophysical conditions and extracted features by using

$$\mathbf{F}_k = \mathbf{S}_k - (\mathbf{f}_1 \cdot \mathbf{S}_k)\ \mathbf{f}_1 - \ldots - (\mathbf{f}_{k-1} \cdot \mathbf{S}_k)\ \mathbf{f}_{k-1} \qquad (7)$$

We chose this procedure for transforming spectra and extracting spectral features to allow us to calculate only the necessary features (to the point where D_k is small enough to be less than what one would expect from the errors of the measurement) in a spectral data base in a straight-forward, simple manner.

RESULTS

After registering the TM (5 October 1984) and SIR-B, 22-degree (10 October 1984) data acquired over the Raisin City Test Site, we extracted N values for 150 fields that had associated ground-based measurements. Using the simple method described before, we converted the N-values to reflectance-factor spectra.

Figure 1 shows a display of the derived reflectance factors for all fields for the red-light band (R_3) and the near-infrared band (R_4). Refer to Table 2 for the definitions of the labels in Figure 1. In general, the pattern in Figure 1 agrees with expected values. The line of soils (solid line in the figure) runs along the bottom of the distribution and the green vegetation spectra extend away from this line in the direction of increasing near-infrared reflectance factors. Note that the orchards (symbols A, N, L, and P) define spectral regions that overlap herbaceous land-cover types (C, H, M, G, F, and R).

Figure 2 shows the full concatenated spectra of representative fields (in this figure, the SIR-B reflectance is assigned to an artificial wavelength of 2.9 μm). The reflectances shown in this figure represent the average reflectance factor over the band pass and not at the central wavelength used for the independent variable. These spectra indicate immediately the advantage

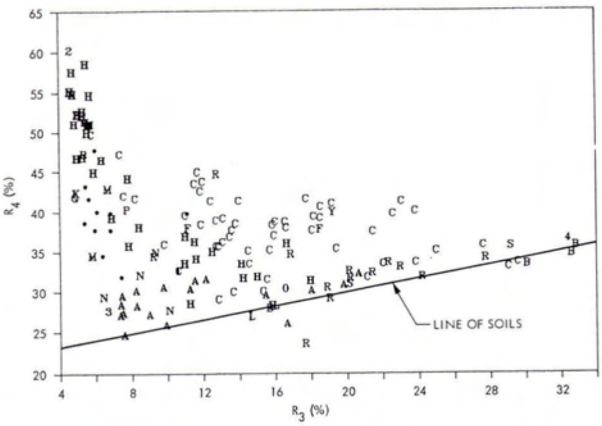

FIG. 1. Near-infrared reflectance (R_4) versus red-light reflectance (R_3) for all fields.

TABLE 2. CODES USED IN FIGURES TO INDICATE GROUND-COVER TYPE.

Code	Meaning
0	Base reference spectrum: cut alfalfa (height, h = 8 cm)
1	1st reference spectrum: mid-cycle alfalfa (h = 15 cm)
2	2nd reference spectrum: mature alfalfa (h = 63 cm)
3	3rd reference spectrum: mature almond orchard
4	4th reference spectrum: dry, smooth bare field
A	Almond orchard
B	Bare field
C	Cotton field
F	Fallow field
G	Fall-planted spring small Grains field
H	Alfalfa (Hay) field
K	Field of oaKs
L	PLum orchard
M	Corn (Maize) field
N	WalNut Orchard
P	Peach orchard
R	PastuRe field
S	Stubble field
Y	BlackeYes field
*	Changed corn field: Corn (5 Oct 86) – Bare (10 Oct 85)

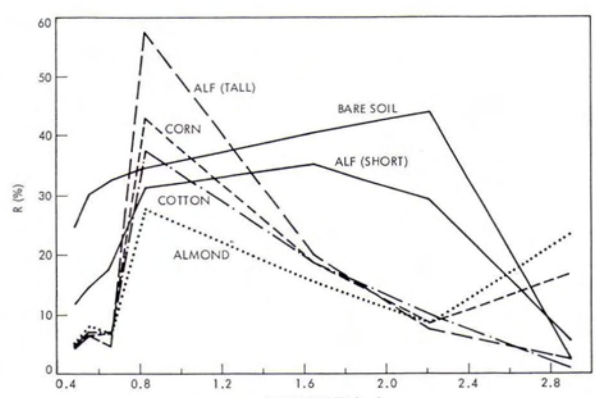

FIG. 2. Concatenated reflectance spectra for selected ground-cover types.

of having concatenated spectra (i.e., data from multiple sensors operating in different parts of the electromagnetic spectrum). The bare-field spectra indicate that the field is dry (see TM Bands 5 and 7) and somewhat smooth (to the radar, see SIR-B Band 8). Compared to bare soil and to short alfalfa, tall alfalfa shows decreases throughout the optical region with stronger decreases in the red-light (TM Band 3) and middle-infrared (TM Bands 5 and 7) portions. At the extreme of the vegetation spectra is the mature alfalfa field that displays very low reflectances in the visible (with the slightly elevated green peak) and in the middle infrared. Again, the microwave backscattering is low. In the near-infrared, R is quite high due to the multiple scattering of light among leaves with the corresponding very low absorption rate. The spectrum of cotton falls into the sequence of alfalfa spectra for the entire range of the concatenated set.

In the optical region, corn has a spectrum similar to intermediate alfalfa; however, in the L-band, the corn field is significantly brighter than the alfalfa fields, the cotton, or the (smooth) bare field. We believe that the enhanced backscatter of microwaves by corn is due to the existence of a well-developed stalk that contains most of the water of a corn plant. In a sense, the corn stalk is more like wood than leaves (herbaceous). Also, the length and even width of the stalk is on the order of the L-band wavelength or larger. Thus, the backscattering by the corn is high due to the dihedreal (corner-like) reflection between the vertical stalk and the horizontal, wet soil surface beneath the corn as appears to be the case for some trees (Richards *et al.*, 1987).

In much of the optical region, the almond spectrum is similar to those of herbaceous plants (alfalfa, cotton, and corn). The only significant departure is the somewhat reduced reflectance in the near-infrared. At this wavelength, the transmission of light by the stems (trunks and branches) is nil while leaves transmit about 50 percent of the light that falls on them. The high leaf reflectance and high transmittance (coupled with low absorptance) led to the high canopy reflectance in this band. The introduction of opaque elements (stems) into the canopy volume leads to greatly reduced canopy reflectance. Nevertheless, the almond spectrum in Figure 2 is similar to the various herbaceous plants. Some of the orchard spectra matched herbaceous spectra closer than the one shown in Figure 2. The greatest difference between the orchards (a combination of woody and herbaceous vegetation) and purely herbaceous vegetation is in the SIR-B band. We shall explore this difference and will expound upon its importance later.

To carryout the operations in the progressive transformation method, we chose the spectrum of recently cut alfalfa for the base spectrum, $\mathbf{R}_B$. For $\mathbf{R}_1$ and $\mathbf{R}_2$, we chose the spectra of mid-cycle alfalfa and mature alfalfa, respectively. With these spectra, we calculated the values of F_1 and F_2 for each field as shown in Figure 3. The base vector, $\mathbf{R}_B$, is

$$\mathbf{R}_B = [11.3\% \quad 14.4\% \quad 16.6\% \quad 30.4\% \quad 33.7\% \quad 29.0\% \quad 1.82\%]^T \tag{8}$$

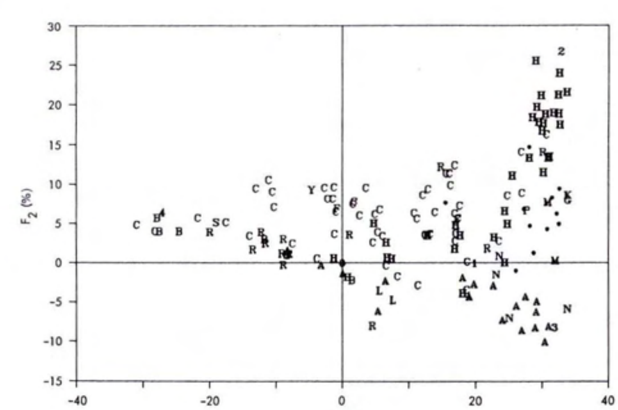

FIG. 3. Distribution of spectra in F_2-F_1 feature space for all fields.

The corresponding unit vectors are

$$\mathbf{f}_1 = [-0.19 \quad -0.20 \quad -0.30 \quad +0.12 \quad -0.53 \quad -0.73 \quad +0.08]^{\mathrm{T}} \tag{9}$$

and

$$\mathbf{f}_2 = [-0.03 \quad -0.05 \quad -0.08 \quad +0.97 \quad +0.14 \quad +0.10 \quad -0.11]^{\mathrm{T}}. \tag{10}$$

One may think of the magnitudes of the various components as being an indication of the relative importance of a given band to the overall extracted spectra feature. In this context, the first extracted spectral feature, F_1, depends on the correlated decreases in reflectances in visible and middle-infrared bands with no significant contributions by the near-infrared or by the L-band microwave reflectance. The second extracted spectra feature, F_2, depends almost exclusively on the increase in the near-infrared reflectance with little influence from the other bands including the SIR-B.

Note that the ranges of F_1 and F_2 in Figure 3 are significantly larger than in the two-band plot before (Figure 1). This is due to the fact that we view the plane of herbaceous vegetation (called the plane of vegetation by Crist and Cicone (1984)) "head on" with the extracted features and obliquely with R_3 and R_4 only. Also, the orchard spectra have rotated slightly away from the other spectra (in Figure 4 compared to Figure 1).

Next, we isolated only the alfalfa spectra in the plot of F_1 versus F_2 (Figure 4). The distribution of the data support the notion that F_1 indicates changes in ground cover. After complete ground cover has been reached, F_2 starts to increase as leaves stack (green leaf area index increases) and multiple scattering effects take hold. The change in alfalfa from freshly cut to mature seems to be tracked by a combination of F_1 and F_2 as might be described by the sweep angle in Figure 4. Comparing the standing height of the alfalfa to the sweep angle (Figure 5) shows that the combination is a good indicator of alfalfa height (and the associated standing green biomass per unit area or green leaf area index).

We calculated the second residual, D_2, of the alfalfa spectra (Figure 6) and found that F_1 and F_2 provide almost all of the information about alfalfa in the data. D_2 is less that 5 percent, a value that we consider to be within the expected error of measurement for the combined set of seven reflectances. Thus, the spectral nature of alfalfa in the concatenated set is essentially two-dimensional, a reduction in dimensionals from seven to two. However, an examination D_2, for all spectra (Figure 7) shows that much information remains in the other spectra, especially in woody vegetation, bare soil, and senescing cotton.

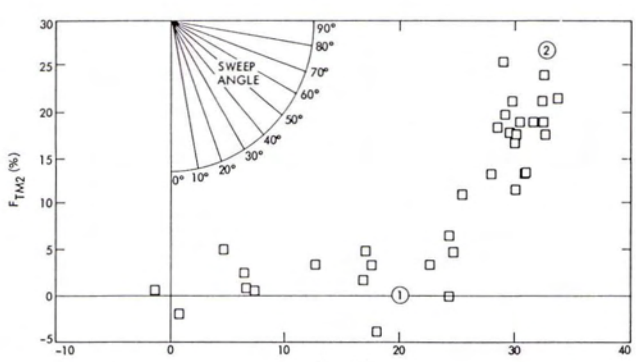

FIG. 4. Distribution of spectra in F_2-F_1 feature space for alfalfa fields.

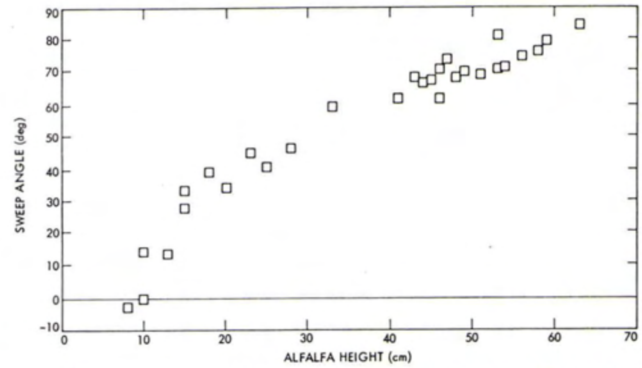

FIG. 5. Sweep angle (combination of F_1 and F_2) versus alfalfa height.

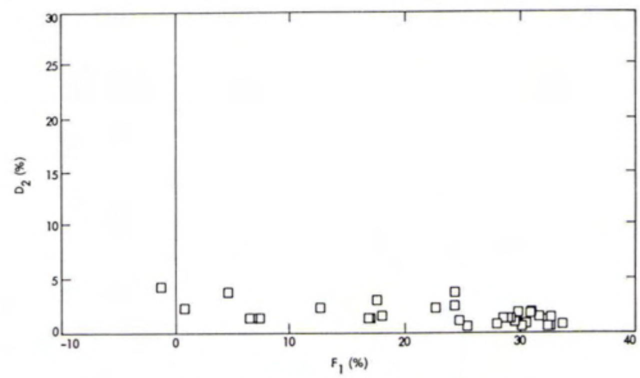

FIG. 6. Second residual (D_2) for alfalfa fields.

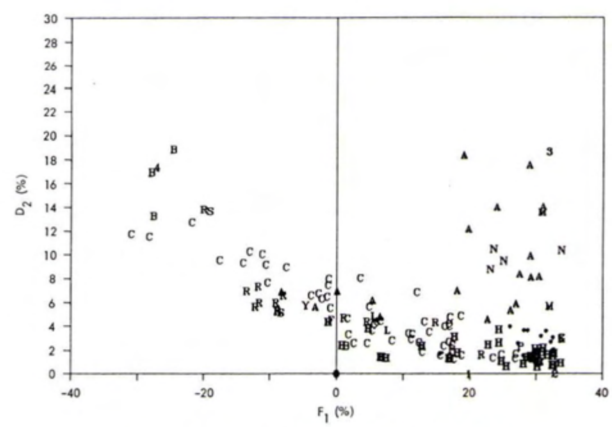

FIG. 7. Second residual (D_2) for all fields.

For the third reference spectrum, we choose a mature almond orchard. The corresponding unit vector was

$$\mathbf{f}_3 = [-0.03 \quad -0.09 \quad -0.05 \quad +0.08 \quad -0.02 \quad +0.19 \quad +0.97]^{\mathrm{T}} \tag{11}$$

The components of $\mathbf{f}_3$ show clearly the dominance of the SIR-B band on the third extracted spectral feature, F_3. Plots of F_3 versus either F_1, F_2, or the sweep angle (F_1-F_2 combination) show that F_3 indicates a biophysical property of woody vegetation in an independent manner (Figure 8). Note the woody nature of corn. Between 5 and 10 October, several corn fields were harvested. Because these were used for sillage, the entire aboveground portion of the corn plant is removed during harvest. Thus, to the radar, these crossover corn plants (indicated by *'s

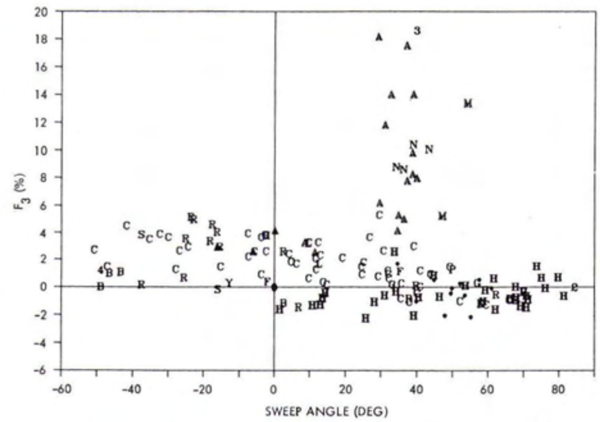

FIG. 8. Distribution of spectra in F_3 sweep-angle space for all fields.

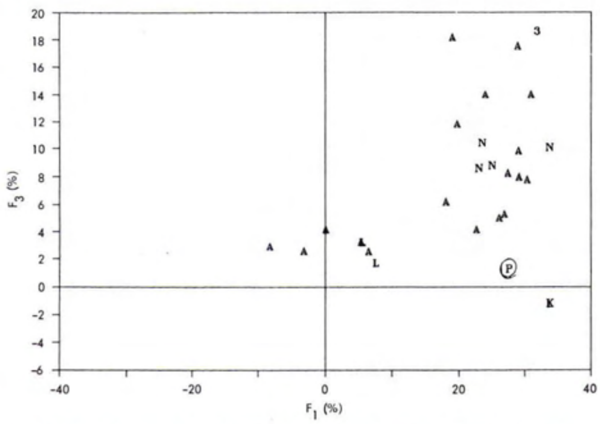

FIG. 9. Distribution of spectra in F_3-F_1 space for orchards.

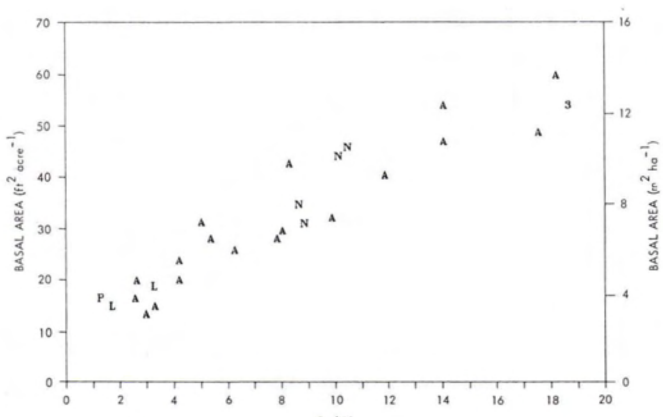

FIG. 10. Basal area of orchards versus F_3.

in the scatter plots) were dark as bare soil or herbaceous plants on 10 October when the SIR-B data were acquired. Figure 9 shows only the orchards in $F_3 - F_1$ space. The oak field (symbol K) was an area with a very sparse cover of oak trees and a grass ground cover. The spectrally nearby peach orchard (symbol P) was also young with a grassy ground cover.

A plot of the basal area, B, of the orchard trees versus F_3 (Figure 10) indicates that F_3 is responding in an almost linear fashion to differences in woody biomass per unit area. Note that, because orchard trees are uniform in age and planting density, a good relationship exists between B and standing biomass per unit area. In a natural forest, one would not expect standing biomass to be related as well to B because natural forest stands contain trees of a wide range of ages and sizes. For the latter, one should use allometric or regression equations that predict the components of standing biomass for each tree based on its diameter (at breast height) and its height. Furthermore, one may find a different relationship between backscatter and B than indicated in Figure 10 when other trees and forests are considered due to variations in the sizes of trunks, stems, and leaves as well as in the condition of the substrate. Sader (1987) found that the relationship between backscatter and standing woody biomass was linear (as in this study) for low biomass values, but approached constant values of backscatter (saturation) for high biomass values. The task before the remote-sensing community is to determine where a useful linear response occurs and where it does not occur as a function of radar wavelength, polarization, and incidence angle. Nevertheless, the results in Figure 10 for orchards are encouraging for the potential use of SAR for woody biomass assessment.

A examination of the third residual, D_3, showed that only the bare soil and defoliated cotton spectra differed from the three-dimensional hyperplane spectral region defined by F_1, F_2, and F_3 (Figure 11). The use of a bare soil spectrum accounted for this variation (data not shown).

CONCLUSIONS

Based on combined Thematic Mapper (TM) and Shuttle Imaging Radar (SIR-B) synthetic aperture radar (SAR) image data over Fresno County, California in October 1984, we found that the sensors provided quantitative information on the amounts of herbaceous and woody vegetation in a given field or area. As expected, the optical reflectance-spectra responded to green biomass per unit area. The L-band HH 22-degree incidence angle SAR data responded to woody components. The combination provides two important indicators of biophysical condition. We used a simple progressive transformation method to translate and rotate the spectral-feature space (concatenated optical and active-microwave data) to isolate three continuous measures or extracted spectral features that indicated percent ground cover of green vegetation, the build up of green biomass (stacking of leaves to generate green leaf area indices greater that unity), and the amount of woody biomass per unit area, respectively. Furthermore, the response of F_3 (controlled primarily by changes in SAR brightness) to woody biomass per unit area (as indicated by basal area) was linear over the range presented by the orchards in the test site. The reader should be careful here not to draw a general conclusion; other studies

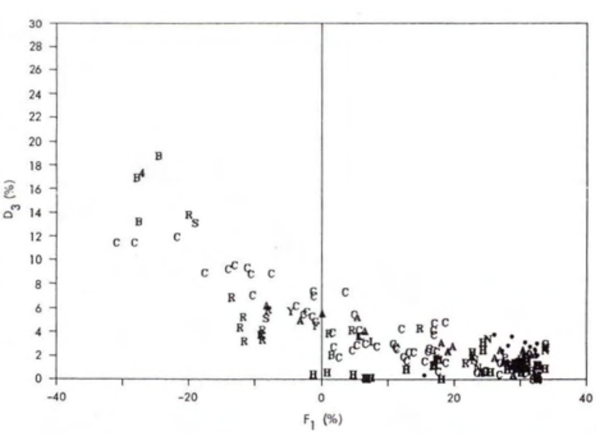

FIG. 11. Third residual (D_3) for all fields.

have shown a saturating response (i.e., little sensitivity to changes in biomass) for high biomass conditions. The authors suggest here that such saturation phenomena may be relieved by the use of even longer wavelengths (such as the P-band on the current NASA airborne SAR). As expected, a combination of F_1, and F_2 (the sweep angle) related well to differences in alfalfa standing height.

The separation of above-ground biomass into herbaceous and woody components is important for many applications. For assessing the effects of land-surface characteristics on climate, one needs these separate categories of information to predict photosyntheses and related gas exchange rates (transpiration, oxygen, and carbon dioxide) from estimates of the rate of absorption of photosynthetically active radiation (APAR). Respiration rates are dependent on the total biomass. Thus, the assessment of net primary production requires the separate assessment of green foliar biomass and woody biomass because these are not well correlated, especially in forests. The existance of woody biomass implies a biomass structure that will influence biosphere/atmosphere interactions through the differential rates of momemtum transfer (drag). The rate of exchange of carbon in plants is much faster when it is stored in leaves as compared to its storage in the woody components. Also, the knowledge of these two basic components of biomass will aid in the process of identifying the type of vegetation. Forests extract water from deeper zones in the soil than herbaceous plants. Thus, the addition of L-band SAR data to more traditional optical scanner information should improve the performance of ecological models over optical or radar alone.

In the future, SAR data will be multiband, multitemporal, multipolarization, and multiangle. These types of data will be available from spacecraft in the early 1990s through the SIR-C, the First European Remote Sensing Satellite (ERS-1) SAR, and the First Japanese Earth Resources Satellite (JERS-1) SAR. Eventually, the data will be provided on a continuing basis in the Earth Observation System (EOS) era. We anticipate the provision of information on the geometric structure of vegetation from multipolarization and multiband SARs and on the nature of the substrate (i.e., bright areas caused by corner reflection) with multiangle SAR.

ACKNOWLEDGMENT

This research was supported by NASA under Contract NAS-700 with the Jet Propulsion Laboratory.

REFERENCES

Cimino, J. B., E. Elachi, and M. Settle, 1986. SIR-B – The second Shuttle Imaging Radar experiment. *IEEE Trans. Geosci. and Remote Sensing*, GE-24(4):445–452.

Colwell, R. N. (ed.), 1983. *Manual of Remote Sensing, 2nd Ed.*, Am. Soc. of Photogrammetry, Washington D.C., 2440 p.

Crist, E. P., and R. C. Cicone, 1984. A physically-based transformation of Thematic Mapper data – the TM Tasseled Cap. *IEEE Trans. Geosci. and Remote Sensing*, GE-22(3):256–267.

Dobson, M. C., F. T. Ulaby, D. R. Brunfeldt, and D. N. Held, 1986. External calibration of SIR-B imagery with area-extended and point targets. *IEEE Trans. on Geosci. and Remote Sensing*, GE-24(4):453–461.

Kauth, R. J., and G. S. Thomas, 1976. The Tasseled Cap – A graphic description of the spectral-temporal development of agricultural crops as seen by Landsat. *Proc. Symp. on Machine Processing of Remotely Sensed Data*, Laboratory of Applications of Remote Sensing, Purdue Univ., West Lafayette, Indiana, pp. 41–51.

Perry, C. R., Jr., and L. F. Lautenschlagar, 1984. Functional equivalence of spectral vegetation indices. *Remote Sensing of Environment*, 14:169–182.

Richards, J. A., G. Q. Sun, and D. S. Simonett, 1987. L-band radar backscatter modelling of forest stands. *IEEE Trans. Geosci. and Remote Sensing*, GE-25, 487–498.

Sader, S. A., 1987. Forest biomass, canopy structure, and species composition relationships with multipolarization L-band synthetic aperture radar data. *Photogrammetric Engineering and Remote Sensing*, 53(2), 193–202.

Sellers, P. J., Y. Mintz, Y. C. Sud, and A. Dalcher, 1986. A simple biosphere model (SiB) for use within general circulation models. *J. Atmos. Sci.*, 43(6):505–531.

Tucker, C. J., 1979: Red and photographic infrared linear combinations for monitoring vegetation. *Remote Sensing of Environment*, 8:127–150.

Wang, J. R., E. T. Engman, J. C. Shiue, M. Rusek, and C. Steinmeier, 1986. The SIR-B observations of microwave backscatter dependence on soil moisture, surface roughness, and vegetation covers. *IEEE Trans. on Geosci. and Remote Sensing*, GE-24(4):517–526.

Wu, S. T., 1981. *Analysis of Results Obtained from Integration of Landsat Multlispectral Scanner and Seasat Synthetic Aperture Radar Data*. Earth Resources Lab., Natl. Instit. of Space Tech., Report No. 189, NSTL Station, Mississippi, 73 p.

(Received 4 October 1987; revised and accepted 19 April 1988)